

Kinetically Coupled Scalar Fields Model and Cosmological Tensions

Gang Liu,[★] Zhihuan Zhou, Yuhao Mu and Lixin Xu[†]

Institute of Theoretical Physics

School of Physics

Dalian University of Technology

Dalian 116024, People's Republic of China

Accepted XXX. Received YYY; in original form ZZZ

ABSTRACT

In this paper, we investigate the kinetically coupled early dark energy (EDE) and scalar field dark matter to address cosmological tensions. The EDE model presents an intriguing theoretical approach to resolving the Hubble tension, but it exacerbates the large-scale structure tension. We consider the interaction between dark matter and EDE, such that the drag of dark energy on dark matter suppresses structure growth, which can alleviate large-scale structure tension. We replace cold dark matter with scalar field dark matter, which has the property of suppressing structure growth on small scales. We employed the Markov Chain Monte Carlo method to constrain the model parameters, our new model reveals a non-zero coupling constant of 0.030 ± 0.026 at a 68% confidence level. The coupled model yields the Hubble constant value of $72.38_{-0.82}^{+0.71}$ km/s/Mpc, which resolves the Hubble tension. However, similar to the EDE model, it also obtains a larger S_8 value compared to the Λ CDM model, further exacerbating the large-scale structure tension. The EDE model and the new model yield the best-fit values of 0.8316 and 0.8146 for S_8 , respectively, indicating that the new model partially alleviates the negative effect of the EDE model. However, this signature disappears when comparing marginalised posterior probabilities, and both models produce similar results. The values obtained from the EDE model and the new model are $0.822_{-0.0093}^{+0.011}$ and $0.819_{-0.0092}^{+0.013}$, respectively, at a 68% confidence level.

Key words: cosmological parameters – dark energy – dark matter

1 INTRODUCTION

The standard Λ CDM model established over the past decades has received significant support from cosmological data. However, with the continuous improvement of experimental measurements, inconsistencies between some observational results and the predicted results of the Λ CDM model have become apparent. The most well-known inconsistencies are the Hubble tension and the large-scale structure tension. The Hubble tension refers to the discrepancy in the value of the Hubble constant derived from early universe observations based on the Λ CDM model and late-time measurements that are independent of the model Verde et al. (2019). Specifically, the best-fit of the Λ CDM model to the *Planck* 2018 cosmic microwave background (CMB) data gives 67.37 ± 0.54 km/s/Mpc Planck Collaboration et al. (2020), whereas the SH0ES collaboration, which uses the distance ladder method at low redshifts, gives 73.04 ± 1.04 km/s/Mpc Riess et al. (2022), with a statistical error of 4.8σ between them.

Another relatively mild tension refers to the inconsistency between the amplitude of density fluctuations σ_8 measured from large-scale structure observations and that measured from CMB observations Macaulay et al. (2013); Hildebrandt et al. (2020). The quantity $S_8 \equiv \sigma_8 \sqrt{(\Omega_m/0.3)}$ is commonly defined to characterise this tension, where Ω_m denotes the matter energy density fraction. The *Planck* 2018 best-fit Λ CDM model yields a value of S_8 equal to

0.834 ± 0.016 Planck Collaboration et al. (2020). However, large-scale structure surveys such as the Dark Energy Survey Year-3 (DES-Y3) have reported a smaller value 0.776 ± 0.017 Abbott et al. (2022).

Currently, it is unclear whether these two tensions stem from unknown statistical errors or inappropriate calibrations Blanchard & Ilić (2021); Mörtzell et al. (2022), for instance, the potential presence of crowding effects in the Cepheid photometry Freedman & Madore (2023), as well as the inaccuracy in the colour/dust correction of type Ia supernovae within calibration galaxies Wojtak & Hjorth (2022); or herald new physics beyond the standard model. In any case, it is still meaningful to explore alternative models to the Λ CDM model and investigate dark matter, dark energy, or dark radiation models that can alleviate these tensions.

Numerous approaches have been proposed to address the Hubble tension, which can be mainly classified into two categories: modifying the physics of the late Universe Guo et al. (2019); Li & Shafieloo (2019); Zhou et al. (2022); Liu et al. (2023d) and introducing new physics prior to recombination Karwal & Kamionkowski (2016); Poulin et al. (2018); Alexander & McDonough (2019); Lin et al. (2019); Berghaus & Karwal (2020); Ghosh et al. (2020); Liu et al. (2023a,b). However, these methods are confronted with various challenges. For instance, the late-time models are competitively constrained by independent observations at low redshift and generally cannot account for SH0ES measurements Benevento et al. (2020); Raveri (2020); Alestas & Perivolaropoulos (2021). Early-time models that achieve relative success in increasing H_0 often exacerbate the tension in large-scale structure Hill et al. (2020); McDonough et al.

[★] E-mail: liugang_dlut@mail.dlut.edu.cn

[†] E-mail: lxxu@dlut.edu.cn

(2022). Despite this, the relative success in relieving Hubble tension through modifications to early universe has stimulated further investigation into such models. In this paper, we will focus on one of the most absorbing cases in early models, namely early dark energy (EDE) model Karwal & Kamionkowski (2016); Lin et al. (2019); Poulin et al. (2019), and address its associated issues.

EDE is composed of an ultra-light scalar field, which only make a significant contribution during the epoch approaching matter-radiation equality, and is negligible during other epochs. The addition of a new component decreases the sound horizon at recombination, thereby allowing an increase in the value of H_0 while keeping the sound horizon angular scale unchanged.

The phenomenological parameter z_c is generally used to represent the redshift at which the energy density of EDE reaches its peak, and f_{EDE} is used to denote the ratio of EDE energy density to the total energy density at this redshift. The value of f_{EDE} reaches approximately 10% can resolve the Hubble tension.

However, obtaining a larger value of H_0 through the EDE scenario comes at the cost of inducing changes in other cosmological parameters, such as the density of dark matter ω_c , the scalar spectral index n_s , and the amplitude of density perturbations σ_8 McDonough et al. (2022). This exacerbates the tension between the model and the large-scale structure data.

One natural idea to address these issues is to introduce the interaction between EDE and dark matter. The drag of dark energy on dark matter can inhibit structure growth, alleviate the large-scale structure tension exacerbated by EDE.

Previous studies have investigated the interaction between EDE and dark matter, such as utilising the Swampland Distance Conjecture Ooguri & Vafa (2007); Klaeuer & Palti (2017); Palti (2019) to consider the exponential dependence of the EDE scalar on the mass of dark matter McDonough et al. (2022); Lin et al. (2023); Liu et al. (2023c). In this work, inspired by string theory, we consider the kinetic coupling between EDE and scalar field dark matter (SFDM).

SFDM, consisting of a light scalar field with a mass of approximately 10^{-22} eV, is a viable alternative to cold dark matter (CDM) Ferreira (2021); Téllez-Tovar et al. (2022). SFDM forms condensates on small scales, which suppress structure growth, while on large scales it exhibits behavior consistent with that of CDM. Fig. 1 illustrates the equation of state evolution with respect to scale factor for SFDM of varying masses. The remaining cosmological parameters adopt the results of the *Planck* 2018 best-fitting Λ CDM model. In the early universe, SFDM behaves like a cosmological constant, then undergoes oscillations before ultimately evolving similarly to CDM, and the mass of the scalar field affects the onset time of the oscillation process.

The kinetic coupling between two scalar fields has been previously investigated, particularly in relation to the axio-dilaton models Alexander & McDonough (2019); Alexander et al. (2023). In this paper, we introduce a EDE scalar-dependent function to the kinetic term of SFDM, allowing for energy exchange between the two scalar fields. The specific Lagrangian is written as

$$\mathcal{L}_{\text{int}} = -\frac{1}{2}g^{\mu\nu}\partial_\mu\phi\partial_\nu\phi - V(\phi) - \frac{1}{2}\zeta(\phi)g^{\mu\nu}\partial_\mu\chi\partial_\nu\chi - V(\chi), \quad (1)$$

where ϕ and χ represent the EDE scalar and SFDM, respectively. The kinetic term of SFDM is multiplied by the coupling function $\zeta(\phi)$.

We conducted a detailed study of the evolution equations for the kinetically coupled scalar fields (KCS) model, including both the background and perturbation parts. We incorporated various commonly used cosmological data, including the *Planck* 2018 CMB

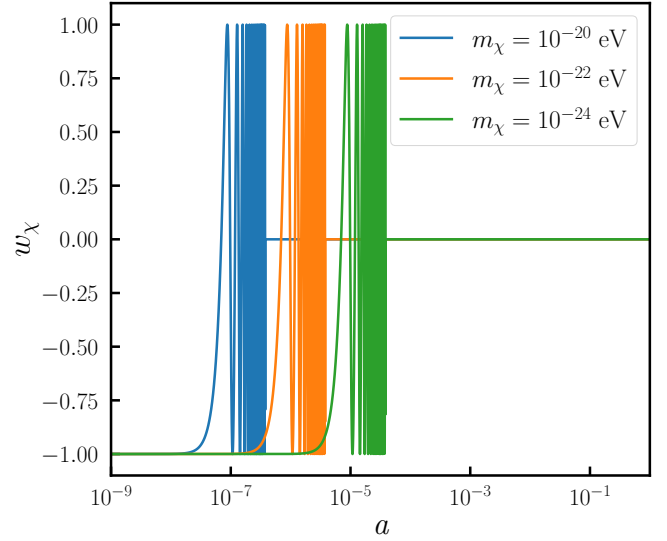


Figure 1. The evolution of the equation of state of scalar field dark matter with respect to the scale factor a is investigated. The evolution of SFDM exhibits behavior similar to a cosmological constant in the early universe, then experiences oscillations, and finally evolves similarly to that of cold dark matter.

temperature, polarization, and lensing measurements Aghanim et al. (2020a,b); Planck Collaboration et al. (2020); BAO measurements from BOSS DR12, 6dF Galaxy Survey, and SDSS DR7 Beutler et al. (2011); Ross et al. (2015); Alam et al. (2017); Buen-Abad et al. (2018); and the Pantheon supernova Ia sample Scolnic et al. (2018). Additionally, we utilised the measurement of the Hubble constant from SHOES Riess et al. (2022) and the results of S_8 from the Dark Energy Survey Year-3 data Abbott et al. (2022).

By employing the Markov Chain Monte Carlo (MCMC) method, we constrained the model parameters. Utilising the entire dataset, the results revealed non-zero coupling constants at a 68% confidence level of 0.030 ± 0.026 . The new model yielded the Hubble constant of $72.38^{+0.71}_{-0.82}$ km/s/Mpc, indicating its capability in addressing the Hubble tension. Similar to the EDE model, the coupling model still obtained a larger S_8 value compared to the Λ CDM model, with the best-fit value being 0.8146. This value is slightly smaller than the result obtained from the EDE model, which is 0.8316. However, when comparing the marginalised posterior probabilities, the results from both models are close. The constrained values of S_8 obtained from the EDE model and the coupled model are $0.822^{+0.011}_{-0.0093}$ and $0.819^{+0.013}_{-0.0092}$, respectively, at a 68% confidence level.

The structure of this paper is as follows: Section 2 introduces the KCS model, discussing its dynamics in both the background and perturbation levels, as well as its modifications to the original EDE model. In Section 3, we present the numerical results of the new model, including its impact on the evolution of the Hubble parameter and large-scale structure. Section 4 provides an introduction to the various cosmological data used in the MCMC analysis, along with the resulting parameter constraints. Finally, we summarise our findings in Section 5.

2 KINETICALLY COUPLED SCALAR FIELDS

Considering the Lagrangian shown in equation (1), we employed the potential form of EDE as follows Hill et al. (2020); Smith et al.

(2020),

$$V(\phi) = m_\phi^2 f_\phi^2 [1 - \cos(\phi/f_\phi)]^3 + V_\Lambda, \quad (2)$$

where m_ϕ represents the axion mass, f_ϕ denotes its decay constant, and V_Λ plays the role of a cosmological constant. For SFDM, we assume a simple quadratic potential,

$$V(\chi) = \frac{1}{2} m_\chi^2 \chi^2, \quad (3)$$

with m_χ representing the mass of the SFDM. As for the coupling function, a natural choice is to assume an exponential form,

$$\zeta(\phi) = \exp\left(\frac{\lambda\phi}{M_{pl}}\right), \quad (4)$$

where λ represents a dimensionless constant that characterises the strength of the interaction, and M_{pl} is the reduced Planck mass.

2.1 Background Equations

The equations of motion for the two scalar fields in a flat Friedmann-Robertson-Walker (FRW) metric can be expressed as

$$\ddot{\phi} + 3H\dot{\phi} + V_\phi - \frac{1}{2} \frac{\lambda}{M_{pl}} \exp\left(\frac{\lambda\phi}{M_{pl}}\right) \dot{\chi}^2 = 0, \quad (5a)$$

$$\ddot{\chi} + (3H + \frac{\lambda\dot{\phi}}{M_{pl}})\dot{\chi} + \exp\left(-\frac{\lambda\phi}{M_{pl}}\right) m_\chi^2 \chi = 0, \quad (5b)$$

where the dot denotes the derivative with respect to cosmic time, H is the Hubble parameter, and V_ϕ represents the partial derivative of the EDE potential with respect to ϕ . It is easy to see that for a non-trivial kinetic coupling function $\zeta(\phi)$, the EDE field has a source term proportional to $\dot{\chi}^2$, while the SFDM field has a friction term proportional to $\dot{\phi}$. Therefore, if $\dot{\chi}$ is not equal to zero and the coupling constant λ is positive, energy will be transferred from SFDM to EDE.

The energy density and pressure of SFDM can be expressed as

$$\rho_\chi = \frac{1}{2} \zeta \dot{\chi}^2 + \frac{1}{2} m_\chi^2 \chi^2, \quad (6a)$$

$$p_\chi = \frac{1}{2} \zeta \dot{\chi}^2 - \frac{1}{2} m_\chi^2 \chi^2, \quad (6b)$$

where we abbreviate $\zeta(\phi)$ as ζ . It is convenient to introduce new variables to calculate the motion equation of SFDM Copeland et al. (1998); Ureña-López & Gonzalez-Morales (2016); Cedeño et al. (2017),

$$\sqrt{\Omega_\chi} \sin \frac{\theta}{2} = \frac{\sqrt{\zeta} \dot{\chi}}{\sqrt{6} M_{pl} H}, \quad (7a)$$

$$\sqrt{\Omega_\chi} \cos \frac{\theta}{2} = -\frac{m_\chi \chi}{\sqrt{6} M_{pl} H}, \quad (7b)$$

$$y_1 = \frac{2m_\chi}{H}, \quad (7c)$$

where $\Omega_\chi = \frac{\rho_\chi}{3M_{pl}^2 H^2}$ represents the fraction of the dark matter density. Combining with the Friedmann Equation,

$$\frac{\dot{H}}{H^2} = -\frac{3}{2}(1 + w_t), \quad (8)$$

where w_t represents the total equation of state, defined as the ratio of the total pressure to the total energy density, the evolution equation

for the new variable is thus formulated as,

$$\frac{\dot{\Omega}_\chi}{\Omega_\chi} = 3H(w_t + \cos \theta) + \frac{\lambda\dot{\phi}}{2M_{pl}}(\cos \theta - 1), \quad (9a)$$

$$\dot{\theta} = Hy_1 \exp\left(-\frac{\lambda\phi}{2M_{pl}}\right) - (3H + \frac{\lambda\dot{\phi}}{2M_{pl}}) \sin \theta, \quad (9b)$$

$$\dot{y}_1 = \frac{3}{2} H(1 + w_t) y_1. \quad (9c)$$

If we consider the energy density and pressure of the EDE scalar field,

$$\rho_\phi = \frac{1}{2} \dot{\phi}^2 + V(\phi), \quad (10a)$$

$$p_\phi = \frac{1}{2} \dot{\phi}^2 - V(\phi), \quad (10b)$$

combined with equation (6) and using the equations of motion for both fields, we obtain the following continuity equations,

$$\dot{\rho}_\chi = -3H(\rho_\chi + p_\chi) - \frac{\lambda\dot{\phi}}{2M_{pl}} \rho_\chi (1 - \cos \theta), \quad (11a)$$

$$\dot{\rho}_\phi = -3H(\rho_\phi + p_\phi) + \frac{\lambda\dot{\phi}}{2M_{pl}} \rho_\chi (1 - \cos \theta). \quad (11b)$$

Many coupled dark energy models exhibit this common structure Olivares et al. (2008); Koyama et al. (2009); Mukherjee & Banerjee (2016); Wang et al. (2016); Yang et al. (2017), which guarantees that the total stress tensor is covariantly conserved.

Fig. 2 illustrates the evolution of the EDE scalar (left panel) and the fraction of the EDE energy density to the total energy density (right panel) with respect to the scale factor. We fix the mass of SFDM at 10^{-22} eV and vary the coupling constant, while the other cosmological parameters, including the EDE parameter, are given by equation (23). Slight variations in the amplitude and phase of the evolution of the EDE scalar field are induced by different coupling constants. The sign of the coupling constant determines the direction of energy transfer. Positive coupling constants indicate energy flow from dark matter to dark energy, resulting in an increase in the energy density fraction of EDE, as demonstrated in the right panel of the figure.

2.2 Perturbation Equations

We employ the synchronous gauge to compute the perturbation equations for both EDE and SFDM. The line element is defined as,

$$ds^2 = -dt^2 + a^2(t)(\delta_{ij} + h_{ij})dx^i dx^j. \quad (12)$$

The perturbed Klein-Gordon equation in the Fourier mode are given by

$$\begin{aligned} \ddot{\delta\phi} = & -3H\dot{\delta\phi} - \left[\frac{k^2}{a^2} + V_{\phi\phi} - \frac{1}{2}\left(\frac{\lambda}{M_{pl}}\right)^2 \exp\left(\frac{\lambda\phi}{M_{pl}}\right) \dot{\chi}^2\right] \delta\phi \\ & - \frac{1}{2} \dot{h}\dot{\phi} + \frac{\lambda}{M_{pl}} \exp\left(\frac{\lambda\phi}{M_{pl}}\right) \dot{\chi} \delta\chi, \end{aligned} \quad (13)$$

$$\begin{aligned} \ddot{\delta\chi} = & -(3H + \frac{\lambda\dot{\phi}}{M_{pl}}) \dot{\delta\chi} - \left[\frac{k^2}{a^2} + m_\chi^2 \exp\left(-\frac{\lambda\phi}{M_{pl}}\right)\right] \delta\chi - \frac{1}{2} \dot{h}\dot{\chi} \\ & + \frac{\lambda}{M_{pl}} [m_\chi^2 \chi \exp\left(-\frac{\lambda\phi}{M_{pl}}\right) \delta\phi - \dot{\chi} \delta\phi], \end{aligned} \quad (14)$$

where $V_{\phi\phi}$ represents the second order partial derivative of the EDE potential with respect to ϕ .

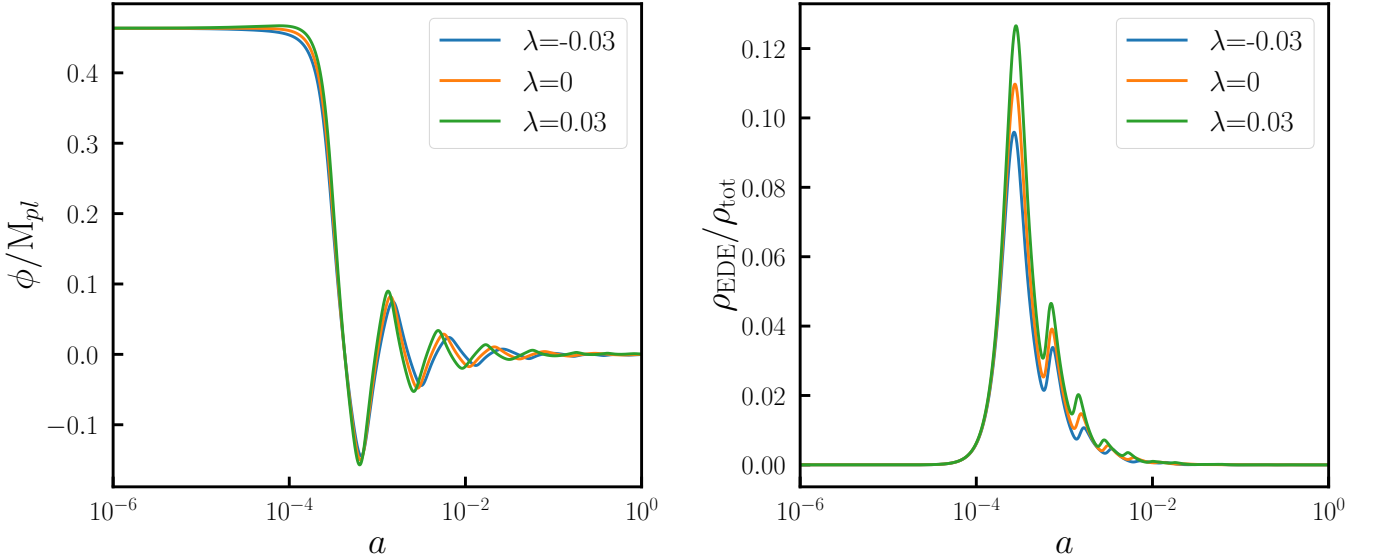


Figure 2. The evolution of the EDE scalar (left panel) and the EDE energy density fraction (right panel) with respect to the scale factor is presented. The amplitude and phase of the EDE scalar are modulated by different coupling constants. Positive coupling constants indicate that energy flows from dark matter to dark energy, thereby increasing the energy density fraction of EDE, while negative coupling constants lead to a decrease in the energy density fraction of EDE.

According to [Ferreira & Joyce \(1998\)](#); [Hu \(1998\)](#), the density perturbation, pressure perturbation, and velocity divergence of SFDM can be expressed as,

$$\delta\rho_\chi = \zeta\dot{\chi}\delta\dot{\chi} + m_\chi^2\chi\delta\chi, \quad (15a)$$

$$\delta p_\chi = \zeta\dot{\chi}\delta\dot{\chi} - m_\chi^2\chi\delta\chi, \quad (15b)$$

$$(\rho_\chi + p_\chi)\Theta_\chi = \frac{k^2}{a}\zeta\dot{\chi}\delta\chi. \quad (15c)$$

We employ some new variables to compute the perturbation equations of SFDM [Cedeño et al. \(2017\)](#),

$$\sqrt{\Omega_\chi}(\delta_0 \sin \frac{\theta}{2} + \delta_1 \cos \frac{\theta}{2}) = \sqrt{\frac{2}{3}} \frac{\sqrt{\zeta}\delta\dot{\chi}}{M_{pl}H}, \quad (16a)$$

$$\sqrt{\Omega_\chi}(\delta_1 \sin \frac{\theta}{2} - \delta_0 \cos \frac{\theta}{2}) = \sqrt{\frac{2}{3}} \frac{m_\chi\delta\chi}{M_{pl}H}. \quad (16b)$$

One can derive the evolution equation for the new variable,

$$\begin{aligned} \dot{\delta}_0 = & -\frac{\lambda Hy_1\delta\phi}{2M_{pl}\sqrt{\zeta}} \sin\theta - \left(\frac{\lambda\delta\phi}{M_{pl}} + \frac{1}{2}\dot{h}\right)(1 - \cos\theta) \\ & + \delta_0 H\omega \sin\theta - \delta_1 \left[(3H + \frac{\lambda\dot{\phi}}{2M_{pl}}) \sin\theta + H\omega(1 - \cos\theta) \right], \end{aligned} \quad (17)$$

$$\begin{aligned} \dot{\delta}_1 = & -\frac{\lambda Hy_1\delta\phi}{2M_{pl}\sqrt{\zeta}} (1 + \cos\theta) - \left(\frac{\lambda\delta\phi}{M_{pl}} + \frac{1}{2}\dot{h}\right) \sin\theta \\ & + \delta_0 H\omega (1 + \cos\theta) - \delta_1 \left[(3H + \frac{\lambda\dot{\phi}}{2M_{pl}}) \cos\theta + H\omega \sin\theta \right], \end{aligned} \quad (18)$$

where

$$\omega = \frac{k^2\sqrt{\zeta}}{2a^2m_\chi H} = \frac{k^2\sqrt{\zeta}}{a^2H^2y_1}. \quad (19)$$

The relationship between the density perturbations, pressure perturbations, and velocity divergence of SFDM and the new variables can

be deduced from equation (15),

$$\delta\rho_\chi = \rho_\chi\delta_0, \quad (20a)$$

$$\delta p_\chi = \rho_\chi(\delta_1 \sin\theta - \delta_0 \cos\theta), \quad (20b)$$

$$(\rho_\chi + p_\chi)\Theta_\chi = \frac{k^2\sqrt{\zeta}}{aHy_1}\rho_\chi[\delta_1(1 - \cos\theta) - \delta_0 \sin\theta]. \quad (20c)$$

2.3 Initial Conditions

In the early universe, Hubble friction in the scalar fields dominated and both EDE and SFDM were effectively frozen, undergoing a slow-roll process. The initial value of ϕ can be set to zero, the term in the EDE equation containing $\dot{\chi}$ can be neglected during that period. Therefore, the equations of motion for EDE and SFDM simplify to an uncoupled form (the equation for the new variable θ is an exception, and we will address this point later). We introduce the ratio of the initial value of the EDE scalar to the axion decay constant, $\alpha_i = \phi_i/f_\phi$ as the model parameter [Hill et al. \(2020\)](#); [Smith et al. \(2020\)](#). We refer to the initial conditions of uncoupled SFDM and make modifications,

$$y_{1i} = \frac{2m_\chi}{H_0\sqrt{\Omega_r}\alpha_i^{-4}}, \quad \theta_i = \frac{1}{5}y_{1i} \exp\left(\frac{-\lambda\phi_i}{2M_{pl}}\right), \quad (21)$$

where Ω_r represents the energy density fraction of all radiation components at present, and α_i denotes the initial value of the scale factor. It should be noted that due to coupling, the initial value of θ is multiplied by an additional factor, $\exp\left(\frac{-\lambda\phi_i}{2M_{pl}}\right)$. For the derivation of the initial conditions of the original SFDM model, please refer to [Ureña-López & Gonzalez-Morales \(2016\)](#); [Cedeño et al. \(2017\)](#). Based on the current value of the dark matter energy density, we employ the widely used shooting method in the Boltzmann code CLASS¹ [Blas et al. \(2011\)](#); [Lesgourgues \(2011\)](#) to obtain the initial value of Ω_χ .

¹ <http://class-code.net>

For the perturbation equations of EDE and SFDM, we employ adiabatic initial conditions, with detailed descriptions provided in [Smith et al. \(2020\)](#) and [Cedeño et al. \(2017\)](#).

3 NUMERICAL RESULTS

Based on the description provided in the previous section, we modified the publicly available Boltzmann code CLASS [Blas et al. \(2011\)](#); [Lesgourgues \(2011\)](#) to incorporate the new model.

We present numerical results using the cosmological parameters borrowed from Table IV in [McDonough et al. \(2022\)](#). More specifically, for the Λ CDM model, we utilise the following parameter values:

$$\omega_b = 0.02258, \quad \omega_{\text{dm}} = 0.1176, \quad (22)$$

$$H_0 = 68.47, \quad \ln(10^{10} A_s) = 3.041,$$

$$n_s = 0.9706, \quad \tau_{\text{reio}} = 0.0535.$$

For the KCS model, we fix the mass of the SFDM at 10^{-22} eV, while varying the coupling constant λ to be 0, -0.03, and 0.03. All other cosmological parameters are chosen based on the results of the EDE model,

$$\omega_b = 0.02281, \quad \omega_{\text{dm}} = 0.1287, \quad (23)$$

$$H_0 = 72.02, \quad \ln(10^{10} A_s) = 3.065,$$

$$n_s = 0.9895, \quad \tau_{\text{reio}} = 0.0581, \quad \alpha_i = 2.77,$$

$$\log_{10}(f_\phi) = 26.61, \quad \log_{10}(m_\phi) = -27.31.$$

We present in Fig. 3 the evolution of the differences in the Hubble parameter between the KCS model and the Λ CDM model for various coupling constants with redshift. The Λ CDM model is depicted by the black dotted line, while the results for the KCS model with coupling parameters 0, -0.03, and 0.03 are represented by the blue solid, orange dashed, and green dash-dotted lines, respectively.

The presence of an early dark energy component in the KCS models leads to higher values of the Hubble parameter compared to the Λ CDM model. Different coupling constants further influence the evolution of the Hubble parameter, with positive coupling constants indicating a transfer of energy density from dark matter to dark energy, resulting in an increase in the EDE energy density fraction (as shown in Fig. 2), leading to a larger Hubble parameter near the critical redshift z_c . Conversely, negative coupling constants have the opposite effect, reducing the Hubble parameter.

Fig. 4 illustrates the redshift evolution of $f\sigma_8$. The 63 observed Redshift Space Distortion $f\sigma_8(z)$ data points are gathered from [Kazantzidis & Perivolaropoulos \(2018\)](#). The KCS models yield higher $f\sigma_8$ compared to the Λ CDM model, exacerbating the existing S_8 tension. This primarily stems from the effects of the EDE component in the KCS model. However, when the coupling constant is non-zero, indicating an interaction between dark matter and dark energy, this result can change. In the case of a positive coupling constant (green dash-dotted line), the value of $f\sigma_8$ is less than the result when the coupling constant is zero (blue solid line), while the effect is opposite when the coupling constant is negative (orange dashed line).

In Fig. 5, we present the linear matter power spectra for various models (top panel) and the differences between the power spectra of KCS model relative to the Λ CDM model (bottom panel).

Similar to previous discussions, the EDE component in the KCS model amplifies the matter power spectrum on small scales, exacerbating the large-scale structure tension. However, the interaction

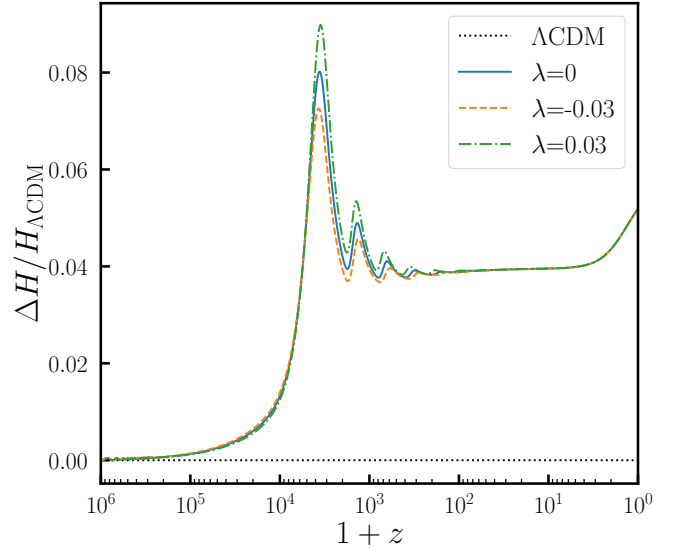


Figure 3. The evolution of the difference in the Hubble parameter between the KCS model and the Λ CDM model with redshift. The inclusion of an early dark energy component in the KCS models results in higher values of the Hubble parameter compared to the Λ CDM model. Furthermore, distinct coupling constants further influence the evolution of the Hubble parameter. Negative coupling constants decrease the Hubble parameter, while positive coupling constants increase it.

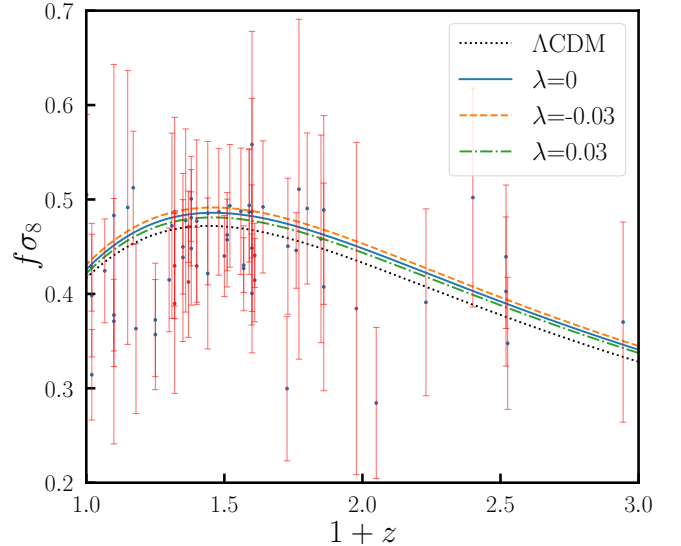


Figure 4. The redshift evolution of $f\sigma_8$ for the various models is examined. In the KCS model, the impact of the EDE component leads to a higher value of $f\sigma_8$ compared to the results obtained within the Λ CDM model. However, when the coupling constant is non-zero (indicating the existence of interaction between dark matter and dark energy), it serves to amend this effect. A positive value of the coupling constant mitigates the adverse effects introduced by EDE.

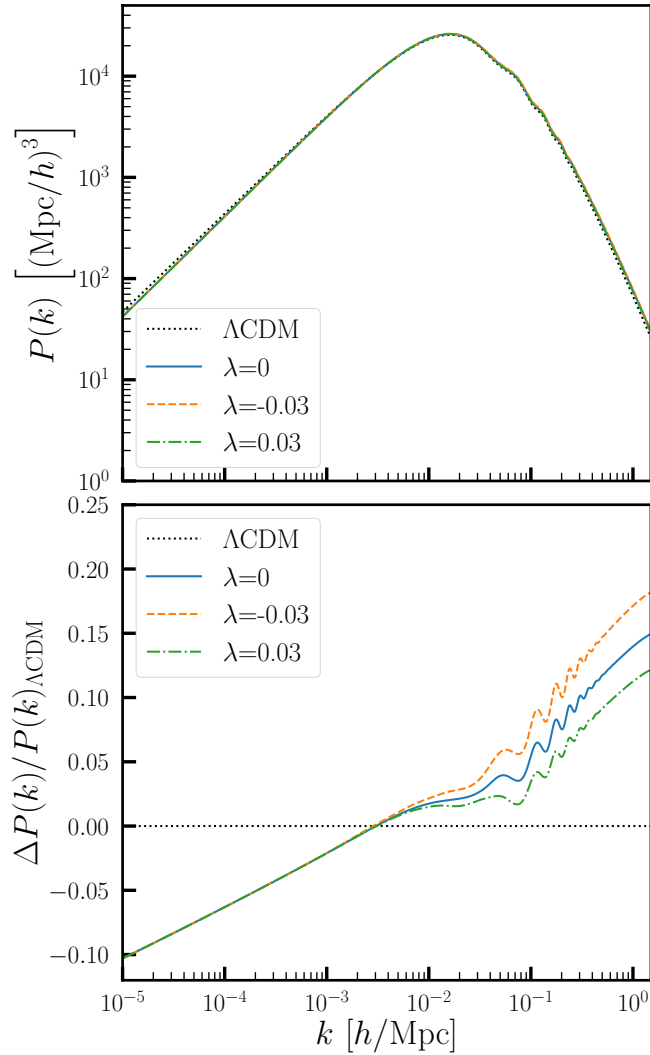


Figure 5. The linear matter power spectra of various models (top panel) and their deviations from the Λ CDM model (bottom panel) are presented. The EDE component in the KCS model increases the matter power on small scales, but the interaction between dark matter and dark energy modifies this result, with positive coupling constants reducing this effect.

between dark matter and dark energy can rectify this outcome. A positive coupling constant leads to the flow of dark matter energy density towards dark energy, suppressing the growth of matter structure and resulting in a smaller power spectrum on small scales.

4 DATA AND METHODOLOGY

We conducted the Markov Chain Monte Carlo (MCMC) analysis using MontePython² Audren et al. (2013); Brinckmann & Lesgourgues (2018) to obtain the posterior distribution of the model parameters. The MCMC chains were analysed using GetDist³ Lewis (2019).

² https://github.com/baudren/montepython_public

³ <https://github.com/cmbant/getdist>

4.1 Datasets

To perform the MCMC analysis, we used the following datasets:

1. **CMB:** The temperature and polarization power spectra obtained from the *Planck* 2018 low- ℓ and high- ℓ measurements, as well as the CMB lensing power spectrum Aghanim et al. (2020a,b); Planck Collaboration et al. (2020).
2. **BAO:** The measurements obtained from the BOSS-DR12 $f\sigma_8$ sample comprise the combined LOWZ and CMASS galaxy samples Alam et al. (2017); Buen-Abad et al. (2018), as well as the small- z measurements derived from 6dFGS and the SDSS DR7 Beutler et al. (2011); Ross et al. (2015).
3. **Supernovae:** The Pantheon dataset consists of 1048 supernovae type Ia with redshift values ranging from 0.01 to 2.3 Scolnic et al. (2018).

By combining CMB and BAO data, acoustic horizon measurements can be made at multiple redshifts, breaking geometric degeneracies and constraining the physical processes between recombination and the redshift at which BAO is measured. The supernova data obtained from the Pantheon sample significantly constrains late-time new physics within its measured redshift range.

4. **SH0ES:** According to the latest SH0ES measurement, the value of the Hubble constant is estimated to be 73.04 ± 1.04 km/s/Mpc Riess et al. (2022).
5. **DES-Y3:** The Dark Energy Survey Year-3 has yielded valuable data on weak lensing and galaxy clustering, from which the parameter S_8 has been measured to be 0.776 ± 0.017 Abbott et al. (2022).

We employ the H_0 measurements from SH0ES to alleviate the prior volume effect Smith et al. (2021) and assess the ability of the novel model to mitigate the tension between H_0 local measurement and CMB inference result. Additionally, we incorporate the S_8 data from DES-Y3 to investigate the efficacy of the model in easing the large-scale structure tension.

4.2 Results

The results of parameter constraints are presented in Table 1, where we utilised a comprehensive dataset comprising CMB, BAO, SNIa, SH0ES, and S_8 from DES-Y3 data to individually constrain the Λ CDM, EDE, and KCS models. The upper segment of the table represents the parameters subjected to MCMC sampling, while the lower segment displays the derived parameters.

Firstly, it is noteworthy that the KCS model constrains the coupling constant λ to be 0.030 ± 0.026 at a 68% confidence level, with a best-fit value of 0.0112. This indicates an interaction between dark matter and dark energy, specifically the conversion of dark matter to dark energy.

From the perspective of the Hubble constant, the EDE model and KCS model yield H_0 values of 72.46 ± 0.86 km/s/Mpc and $72.38^{+0.71}_{-0.82}$ km/s/Mpc, respectively, at a 68% confidence level, both of which exceed the value of $68.71^{+0.35}_{-0.41}$ km/s/Mpc obtained by the Λ CDM model. Therefore, both the EDE model and KCS model demonstrate the capacity to address the Hubble tension.

However, the performance of both models on S_8 is suboptimal. The best-fit values of S_8 for the EDE and KCS models are 0.8316 and 0.8146, respectively, whereas Λ CDM yields a result of 0.8016. Both models exacerbate the preexisting S_8 tension. The result obtained from the KCS model is smaller than that from the EDE model, indicating that the new model partially alleviates the negative effect

Table 1. The table illustrates the best-fit parameters and 68% confidence level marginalised constraints for the Λ CDM, EDE, and KCS models. These constraints are derived from comprehensive data sets including CMB, BAO, SNIa, SHOES, and S_8 measurements obtained from DES-Y3. The upper portion of the table consists of the cosmological parameters that were explored using MCMC sampling, while the lower portion presents the derived parameters.

Model	Λ CDM	EDE	KCS
$100\omega_b$	2.260(2.263 \pm 0.014)	2.276(2.281 ^{+0.024} _{-0.020})	2.305(2.281 \pm 0.020)
ω_{dm}	0.11729(0.11725 \pm 0.00084)	0.1310(0.1299 \pm 0.0028)	0.1286(0.1303 \pm 0.0028)
H_0	68.64(68.71 ^{+0.35} _{-0.41})	71.85(72.46 \pm 0.86)	72.71(72.38 ^{+0.71} _{-0.82})
$\ln(10^{10}A_s)$	3.047(3.050 \pm 0.015)	3.057(3.063 ^{+0.015} _{-0.017})	3.069(3.057 \pm 0.018)
n_s	0.9733(0.9722 \pm 0.0040)	0.9877(0.9908 \pm 0.0059)	0.9943(0.9875 ^{+0.0065} _{-0.0041})
τ_{reio}	0.0575(0.0592 \pm 0.0082)	0.0539(0.0563 \pm 0.0090)	0.0614(0.0543 \pm 0.0093)
$\log_{10}(m_\phi)$	–	–27.292(–27.290 \pm 0.055)	–27.241(–27.295 ^{+0.052} _{-0.042})
$\log_{10}(f_\phi)$	–	26.632(26.616 ^{+0.056} _{-0.033})	26.632(26.645 \pm 0.051)
α_i	–	2.762(2.783 \pm 0.069)	2.734(2.696 ^{+0.069} _{-0.055})
λ	–	–	0.0112(0.030 \pm 0.026)
$\log_{10}(m_\chi)$	–	–	–21.980(–21.988 \pm 0.063)
$10^{-9}A_s$	2.105(2.112 \pm 0.032)	2.127(2.139 ^{+0.031} _{-0.036})	2.153(2.127 \pm 0.038)
$100\theta_s$	1.04206(1.04217 ^{+0.00025} _{-0.00031})	1.04121(1.04145 \pm 0.00043)	1.04149(1.04140 ^{+0.00028} _{-0.00039})
f_{EDE}	–	0.1183(0.119 ^{+0.023} _{-0.018})	0.1168(0.124 \pm 0.021)
$\log_{10}(z_c)$	–	3.571(3.568 \pm 0.034)	3.601(3.569 ^{+0.028} _{-0.025})
Ω_m	0.2983(0.2977 \pm 0.0048)	0.2991(0.2923 \pm 0.0056)	0.2880(0.2935 ^{+0.0057} _{-0.0043})
σ_8	0.8039(0.8047 \pm 0.0060)	0.8329(0.8325 \pm 0.0083)	0.8313(0.8284 ^{+0.0088} _{-0.0071})
S_8	0.8016(0.8016 ^{+0.0096} _{-0.0080})	0.8316(0.822 ^{+0.011} _{-0.0093})	0.8146(0.819 ^{+0.013} _{-0.0092})
χ^2_{tot}	3838.20	3826.46	3825.42
ΔAIC	–	–5.74	–2.78

of the EDE model. However, when comparing the marginalised posterior probabilities, this feature vanishes, both models yield similar results. The constrained values of S_8 obtained from the EDE model and the KCS model are $0.822^{+0.011}_{-0.0093}$ and $0.819^{+0.013}_{-0.0092}$, respectively, at a 68% confidence level.

These discussions can be visually depicted in the marginalised posterior distributions of various models, as illustrated in Fig. 6. The complete posterior distributions can be found in Fig. A1 in the Appendix section.

The penultimate row of Table 1 displays the χ^2_{tot} values of the different models. The discrepancies of the EDE and KCS models compared to the Λ CDM model are -11.74 and -12.78, respectively. Both models exhibit significantly reduced χ^2_{tot} values compared to the Λ CDM model, primarily due to the contribution from the SHOES data. Furthermore, the KCS model demonstrates a lower χ^2_{tot} value than the EDE model, attributed to its smaller S_8 value, which better aligns with the DES-Y3 data.

We also calculated the Akaike Information Criterion (AIC) for model comparison Akaike (1974),

$$AIC = \chi^2_{tot} + 2k, \quad (24)$$

where k represents the number of fitting parameters. The results of different models compared to the Λ CDM model are presented in the last row of Table 1. We find that the EDE model has the lowest AIC, followed by the KCS model, both of which yield smaller values than that of the Λ CDM model. This indicates that both models outperform the Λ CDM model. Furthermore, compared to the EDE model, although the KCS model has a smaller χ^2_{tot} value, its introduction of additional parameters makes its performance inferior to that of the EDE model from the perspective of AIC.

Additionally, we conducted a renewed MCMC analysis after ex-

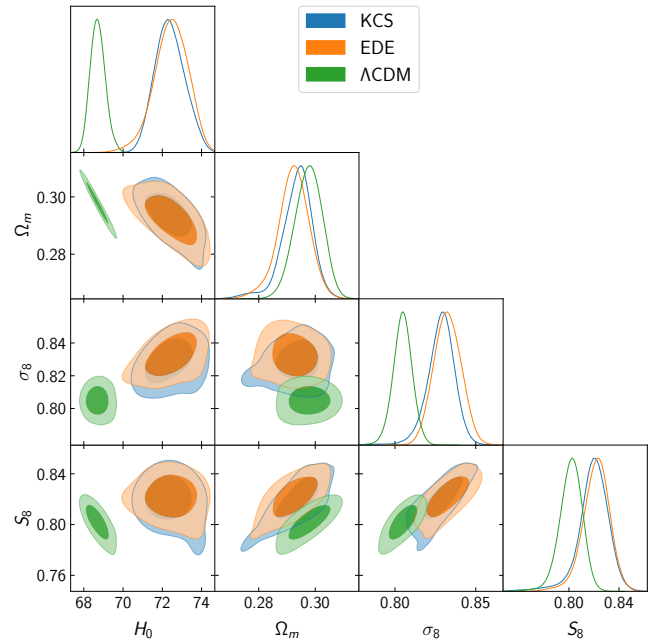


Figure 6. The marginalised posterior distributions of the three models are presented. Both the EDE and KCS models yield larger values of H_0 and hence, a larger S_8 compared to the Λ CDM model. However, the KCS model partially alleviates the S_8 tension when compared to the EDE model.

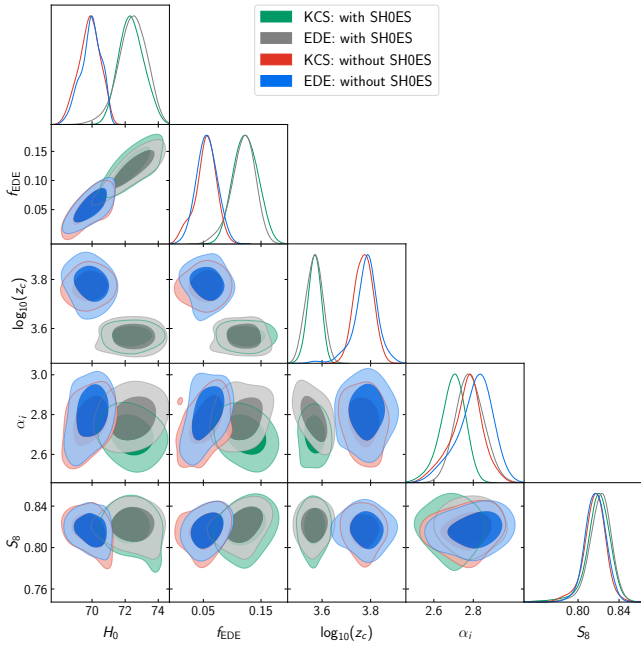


Figure 7. The marginalised posterior distributions of the parameters H_0 , S_8 , and EDE parameters for the KCS and EDE models are derived with and without the inclusion of SH0ES data. After the exclusion of SH0ES data, both models yield very small values for f_{EDE} .

cluding the SH0ES data to investigate its impact on the EDE parameters. Our constrained parameter results are illustrated in Table 2, where the utilised data only consist of CMB, BAO, SNIa, and S_8 measurements obtained from DES-Y3.

We observed that in the absence of SH0ES data, the phenomenological parameters f_{EDE} obtained from the EDE model and KCS model constraints are very small, with best-fit values of 0.0548 and 0.0311, respectively, which are consistent with previous findings Smith et al. (2021); Poulin et al. (2023). It is noteworthy that in our MCMC analysis, we sampled over the axion mass m_ϕ and decay constant f_ϕ , while the EDE parameters f_{EDE} and z_c are derived parameters. As a result, our findings may differ from those of other studies.

In Fig. 7, we present the contour plots of the constraints on the H_0 , S_8 , and EDE parameters for the KCS model and EDE model, with and without the inclusion of SH0ES data.

The impact of the SH0ES data on the EDE parameter is clearly evident. Excluding the SH0ES data leads to a reduction in the EDE parameter f_{EDE} and an associated higher critical redshift z_c , indicating a subtle signal of the existence of EDE. The results obtained from the KCS model and the EDE model are consistent.

In order to quantify the level of tension with the SH0ES data, we computed the following tension metric (in units of Gaussian σ) Raveri & Hu (2019); Schöneberg et al. (2022),

$$Q_{\text{DMAP}} \equiv \sqrt{\chi^2(w/\text{SH0ES}) - \chi^2(w/o \text{SH0ES})}, \quad (25)$$

which calculates the difference in χ^2 when considering with and without SH0ES data. This metric effectively captures the non-Gaussianity of the posterior. The tension metric yields results of 4.4σ , 2.1σ , and 1.8σ for the ΛCDM model, EDE model, and KCS model, respectively (it is noted that our data includes S_8 from DES-Y3, hence yielding slightly different results from previous studies).

According to this criterion, we consider both the EDE model and the KCS model to be superior to the ΛCDM model.

5 CONCLUSIONS

In this paper, we investigate the interaction between early dark energy (EDE) and scalar field dark matter (SFDM), proposing a kinetically coupled scalar fields (KCS) model to alleviate cosmological tensions. The EDE model offers a resolution to the Hubble tension, but exacerbates the S_8 tension.

In light of this, we propose an interaction between dark matter and dark energy, aiming to alleviate the S_8 tension through the drag exerted by dark energy on dark matter.

In particular, motivated by the ability of SFDM to suppress structure growth on small scales, we replace cold dark matter with SFDM. Inspired by string theory, we consider a kinetic coupling between two scalar fields, where the kinetic term of SFDM is multiplied by an EDE scalar-dependent function.

We derived the evolution equations of the KCS model at both the background and perturbation levels, and investigated its impact on the evolution of the Hubble parameter, as well as on the structure growth and matter power spectrum. By using cosmological data from various sources, including the CMB, BAO, SNIa, the SH0ES measurement of the Hubble constant, and the DES-Y3 observations, we conducted the MCMC analysis.

We obtained a non-zero coupling constant λ of 0.030 ± 0.026 at a 68% confidence level. This suggests the interaction between dark matter and dark energy, with energy transferring from dark matter to dark energy. The values of H_0 of the EDE model and KCS model are 72.46 ± 0.86 km/s/Mpc and $72.38^{+0.71}_{-0.82}$ km/s/Mpc, respectively, while the result of ΛCDM model is $68.71^{+0.35}_{-0.41}$ km/s/Mpc. Both models alleviate the Hubble tension.

However, the corresponding cost is that both the EDE model and KCS model yield larger values of S_8 , with their best-fit values being 0.8316 and 0.8146, respectively, which are greater than the result of the ΛCDM model, 0.8016. Compared to the EDE model, the result from the KCS model is smaller, indicating that the new model partially mitigates the negative effect of the original EDE model. However, this feature disappears when comparing the marginalised posterior probabilities, as both models yield similar results. The constrained results for S_8 from the EDE model and the KCS model are $0.822^{+0.011}_{-0.0093}$ and $0.819^{+0.013}_{-0.0092}$, respectively, at a 68% confidence level.

We computed the $\Delta\chi^2_{\text{tot}}$ values of the EDE model and KCS model relative to the ΛCDM model, which are -11.74 and -12.78, respectively. This is primarily attributed to the contribution of SH0ES data. The χ^2_{tot} value of the KCS model is slightly smaller than that of the EDE model, mainly due to the fact that the KCS model yields a smaller S_8 , which aligns better with the DES-Y3 data. We further calculated the AIC to compare the models, and the results indicate that the EDE model has the lowest AIC, followed by the KCS model. The introduction of additional parameters in the KCS model leads to its inferior performance compared to the EDE model.

We also briefly investigated the impact of the SH0ES data on the EDE parameter. When excluding the SH0ES data, the constrained f_{EDE} parameters from both the EDE and KCS models are smaller, suggesting a weak signal of the presence of EDE, consistent with previous findings in the literature.

Building upon the EDE model, we considered the coupling between dark matter and dark energy to mitigate the negative effect inherent in the EDE model. However, the coupled model still falls

Table 2. After excluding SH0ES data, the best-fit values and 68% confidence level marginalised constraints on the parameters of the Λ CDM model, the EDE model, and the KCS model, using only CMB, BAO, SNIa, and S_8 measurements obtained from DES-Y3 data.

Model	Λ CDM	EDE	KCS
$100\omega_b$	2.249(2.252 \pm 0.014)	2.283(2.279 \pm 0.018)	2.257(2.275 \pm 0.020)
ω_{dm}	0.11823(0.11825 \pm 0.00085)	0.1232(0.1230 ^{+0.0020} _{-0.0023})	0.1210(0.1227 ^{+0.0023} _{-0.0021})
H_0	68.11(68.21 \pm 0.39)	69.74(69.94 ^{+0.79} _{-0.49})	68.94(69.85 ^{+0.73} _{-0.62})
$\ln(10^{10}A_s)$	3.045(3.045 \pm 0.017)	3.060(3.055 ^{+0.015} _{-0.019})	3.044(3.050 \pm 0.016)
n_s	0.9699(0.9693 \pm 0.0038)	0.9845(0.9813 ^{+0.0056} _{-0.0048})	0.9714(0.9798 \pm 0.0053)
τ_{reio}	0.0568(0.0563 \pm 0.0080)	0.0594(0.0577 ^{+0.0081} _{-0.010})	0.0531(0.0550 \pm 0.0083)
$\log_{10}(m_\phi)$	–	–26.837(–26.90 ^{+0.10} _{-0.081})	–26.992(–26.909 \pm 0.072)
$\log_{10}(f_\phi)$	–	26.392(26.405 ^{+0.081} _{-0.056})	26.261(26.379 ^{+0.084} _{-0.048})
α_i	–	2.845(2.81 ^{+0.10} _{-0.076})	2.779(2.765 ^{+0.090} _{-0.066})
λ	–	–	0.060(0.032 ^{+0.039} _{-0.028})
$\log_{10}(m_\chi)$	–	–	–22.608(–22.670 \pm 0.059)
$10^{-9}A_s$	2.101(2.102 \pm 0.035)	2.132(2.122 ^{+0.032} _{-0.041})	2.098(2.111 \pm 0.033)
$100\theta_s$	1.04181(1.04204 ^{+0.00027} _{-0.00030})	1.04182(1.04183 ^{+0.00026} _{-0.00041})	1.04192(1.04195 ^{+0.00022} _{-0.00046})
f_{EDE}	–	0.0548(0.056 \pm 0.018)	0.0311(0.054 ^{+0.021} _{-0.015})
$\log_{10}(z_c)$	–	3.810(3.780 ^{+0.050} _{-0.037})	3.725(3.772 \pm 0.038)
Ω_m	0.3047(0.3040 \pm 0.0050)	0.3016(0.2995 ^{+0.0058} _{-0.0047})	0.3034(0.2996 ^{+0.0060} _{-0.0049})
σ_8	0.8055(0.8056 \pm 0.0065)	0.8216(0.8178 \pm 0.0079)	0.8116(0.8168 ^{+0.0064} _{-0.0072})
S_8	0.8118(0.8110 \pm 0.0093)	0.8237(0.817 \pm 0.010)	0.8161(0.816 ^{+0.011} _{-0.0089})
χ^2_{tot}	3818.96	3822.28	3822.18

short of resolving all cosmological tensions, and it is not fully supported by the data. Further efforts are still required to address these challenges comprehensively.

ACKNOWLEDGEMENTS

This work is supported in part by National Natural Science Foundation of China under Grant No.12075042, Grant No.11675032 (People's Republic of China).

DATA AVAILABILITY

The data supporting the findings of this article are available upon reasonable request to the corresponding author.

REFERENCES

Abbott T. M. C., Aguena M., Alarcon A., et al., 2022, *Phys. Rev. D*, 105, 023520

Aghanim N., Akrami Y., Ashdown M., et al., 2020b, *Astronomy and Astrophysics*, 641

Aghanim N., Akrami Y., Ashdown M., et al., 2020a, *Astronomy and Astrophysics*, 641

Akaike H., 1974, *IEEE Transactions on Automatic Control*, 19, 716

Alam S., Ata M., Bailey S., et al., 2017, *Monthly Notices of the Royal Astronomical Society*, 470, 2617

Alestars G., Perivolaropoulos L., 2021, *Monthly Notices of the Royal Astronomical Society*, 504, 3956

Alexander S., McDonough E., 2019, *Physics Letters B*, 797, 134830

Alexander S., Bernardo H., Toomey M. W., 2023, *Journal of Cosmology and Astroparticle Physics*, 2023, 037

Audren B., Lesgourgues J., Benabed K., Prunet S., 2013, *Journal of Cosmology and Astroparticle Physics*, 2013, 001

Benevento G., Hu W., Raveri M., 2020, *Phys. Rev. D*, 101, 103517

Berghaus K. V., Karwal T., 2020, *Phys. Rev. D*, 101, 083537

Beutler F., Blake C., Colless M., et al., 2011, *Monthly Notices of the Royal Astronomical Society*, 416, 3017

Blanchard A., Ilić S., 2021, *Astronomy and Astrophysics*, 656, A75

Blas D., Lesgourgues J., Tram T., 2011, *Journal of Cosmology and Astroparticle Physics*, 2011, 034

Brinckmann T., Lesgourgues J., 2018, MontePython 3: boosted MCMC sampler and other features ([arXiv:1804.07261](https://arxiv.org/abs/1804.07261))

Buen-Abad M. A., Schmaltz M., Lesgourgues J., Brinckmann T., 2018, *Journal of Cosmology and Astroparticle Physics*, 2018, 008

Cedeño F. X. L., González-Morales A. X., Ureña López L. A., 2017, *Phys. Rev. D*, 96, 061301

Copeland E. J., Liddle A. R., Wands D., 1998, *Phys. Rev. D*, 57, 4686

Ferreira E. G. M., 2021, *The Astronomy and Astrophysics Review*, 29

Ferreira P. G., Joyce M., 1998, *Phys. Rev. D*, 58, 023503

Freedman W. L., Madore B. F., 2023, The Cepheid Extragalactic Distance Scale: Past, Present and Future ([arXiv:2308.02474](https://arxiv.org/abs/2308.02474))

Ghosh S., Khatri R., Roy T. S., 2020, *Phys. Rev. D*, 102, 123544

Guo R.-Y., Zhang J.-F., Zhang X., 2019, *Journal of Cosmology and Astroparticle Physics*, 2019, 054

Hildebrandt H., Köhlinger F., Busch J., et al., 2020, *Astronomy & Astrophysics*, 633, A69

Hill J. C., McDonough E., Toomey M. W., Alexander S., 2020, *Phys. Rev. D*, 102, 043507

Hu W., 1998, *The Astrophysical Journal*, 506, 485

Karwal T., Kamionkowski M., 2016, *Phys. Rev. D*, 94, 103523

Kazantzidis L., Perivolaropoulos L., 2018, *Phys. Rev. D*, 97, 103503

Klaewer D., Palti E., 2017, *Journal of High Energy Physics*, 2017

Koyama K., Maartens R., Song Y.-S., 2009, *Journal of Cosmology and Astroparticle Physics*, 2009, 017

Lesgourgues J., 2011, The Cosmic Linear Anisotropy Solving System (CLASS) I: Overview ([arXiv:1104.2932](https://arxiv.org/abs/1104.2932))

Lewis A., 2019, GetDist: a Python package for analysing Monte Carlo samples

- ([arXiv:1910.13970](https://arxiv.org/abs/1910.13970))
- Li X., Shafieloo A., 2019, *The Astrophysical Journal Letters*, 883, L3
- Lin M.-X., Benevento G., Hu W., Raveri M., 2019, *Phys. Rev. D*, 100, 063542
- Lin M.-X., McDonough E., Hill J. C., Hu W., 2023, *Phys. Rev. D*, 107, 103523
- Liu G., Gao J., Han Y., Mu Y., Xu L., 2023a, Mitigating Cosmological Tensions via Momentum-Coupled Dark Sector Model ([arXiv:2310.09798](https://arxiv.org/abs/2310.09798))
- Liu G., Mu Y., Gao J., Han Y., Xu L., 2023b, The Yukawa-Coupled Dark Sector Model and Cosmological Tensions ([arXiv:2312.01410](https://arxiv.org/abs/2312.01410))
- Liu G., Zhou Z., Mu Y., Xu L., 2023c, *Phys. Rev. D*, 108, 083523
- Liu G., Mu Y., Zhou Z., Xu L., 2023d, *Phys. Rev. D*, 108, 123546
- Macaulay E., Wehus I. K., Eriksen H. K., 2013, *Phys. Rev. Lett.*, 111, 161301
- McDonough E., Lin M.-X., Hill J. C., Hu W., Zhou S., 2022, *Phys. Rev. D*, 106, 043525
- Mukherjee A., Banerjee N., 2016, *Classical and Quantum Gravity*, 34
- Mörtsell E., Goobar A., Johansson J., Dhawan S., 2022, *The Astrophysical Journal*, 933, 212
- Olivares G., Atrio-Barandela F., Pavón D., 2008, *Phys. Rev. D*, 77, 063513
- Ooguri H., Vafa C., 2007, *Nuclear Physics B*, 766, 21
- Palti E., 2019, *Fortschritte der Physik*, 67
- Planck Collaboration Aghanim, N. Akrami, Y. et al., 2020, *Astronomy and Astrophysics*, 641, A6
- Poulin V., Smith T. L., Grin D., Karwal T., Kamionkowski M., 2018, *Phys. Rev. D*, 98, 083525
- Poulin V., Smith T. L., Karwal T., Kamionkowski M., 2019, *Phys. Rev. Lett.*, 122, 221301
- Poulin V., Smith T. L., Karwal T., 2023, The Ups and Downs of Early Dark Energy solutions to the Hubble tension: a review of models, hints and constraints circa 2023 ([arXiv:2302.09032](https://arxiv.org/abs/2302.09032))
- Raveri M., 2020, *Phys. Rev. D*, 101, 083524
- Raveri M., Hu W., 2019, *Phys. Rev. D*, 99, 043506
- Riess A. G., et al., 2022, *The Astrophysical Journal Letters*, 934, L7
- Ross A. J., Samushia L., Howlett C., et al., 2015, *Monthly Notices of the Royal Astronomical Society*, 449, 835
- Schöneberg N., Abellán G. F., Sánchez A. P., Witte S. J., Poulin V., Lesgourgues J., 2022, *Physics Reports*, 984, 1
- Scolnic D. M., Jones D. O., Rest A., Pan Y. C., et al., 2018, *The Astrophysical Journal*, 859, 101
- Smith T. L., Poulin V., Amin M. A., 2020, *Phys. Rev. D*, 101, 063523
- Smith T. L., Poulin V., Bernal J. L., Boddy K. K., Kamionkowski M., Murgia R., 2021, *Phys. Rev. D*, 103, 123542
- Téllez-Tovar L. O., Matos T., Vázquez J. A., 2022, *Phys. Rev. D*, 106, 123501
- Ureña-López L. A., Gonzalez-Morales A. X., 2016, *Journal of Cosmology and Astroparticle Physics*, 2016, 048
- Verde L., Treu T., Riess A. G., 2019, *Nature Astronomy*, 3, 891
- Wang B., Abdalla E., Atrio-Barandela F., Pavón D., 2016, *Reports on Progress in Physics*, 79, 096901
- Wojtak R., Hjorth J., 2022, *Monthly Notices of the Royal Astronomical Society*, 515, 2790
- Yang W., Pan S., Mota D. F., 2017, *Phys. Rev. D*, 96, 123508
- Zhou Z., Liu G., Mu Y., Xu L., 2022, *Monthly Notices of the Royal Astronomical Society*, 511, 595

APPENDIX A: THE FULL MCMC POSTERiors

This paper has been typeset from a $\text{\TeX}/\text{\LaTeX}$ file prepared by the author.

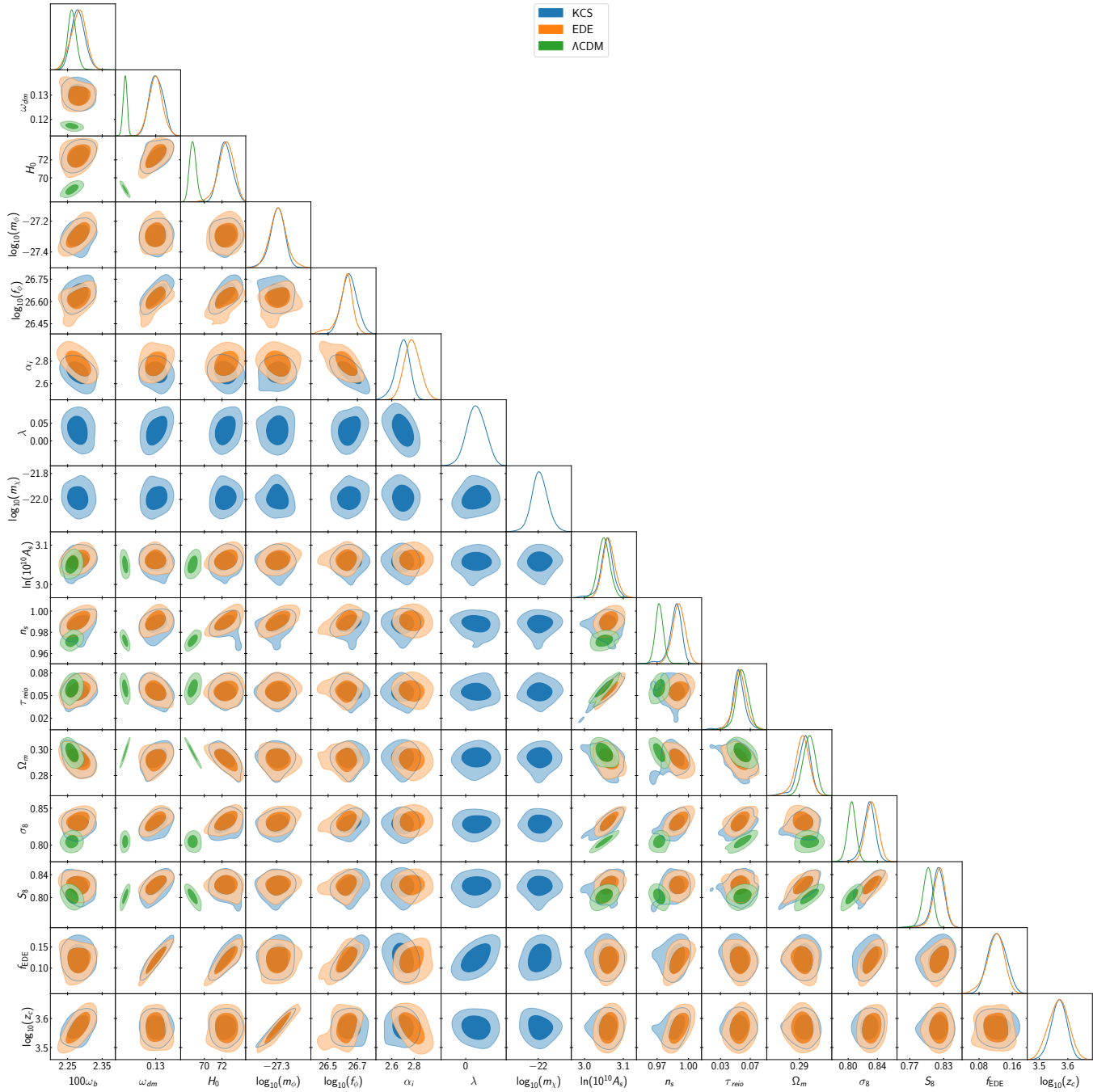


Figure A1. The complete posterior distributions for Λ CDM, EDE, and KCS models with data comprising CMB, BAO, SNIa, SH0ES, and S_8 from DES-Y3.